Glacier Retreat, Outburst Floods, and Kinematic Wave: Long-Term Nisqually Glacier Changes Related to Climate Change

FINAL REPORT: ***June 10, 2016***
TASK AGREEMENT: P12AC15072
COOPERATIVE AGREEMENT: H8W07110001
PI: Howard Conway (University of Washington)

Existing Nisqually Glacier survey data and supporting notes were digitized and compiled to document:

1. Changes in elevation of profiles measured across the glacier during surveys, from 1931 to 2015.
2. The passage of kinematic waves down glacier.
3. Changes of length, area and mass balance of the glacier.

Using these data, as well as climate records from Longmire and Paradise, we modeled the response of Nisqually Glacier to changes in mass balance and explored the sensitivity to changes in temperature and precipitation. We also investigated possible relationships between mass balance, kinematic waves, glacier length, and outburst floods.

Significant results include:

- Climate records from Longmire and Paradise indicate recent (1970 – 2015) warming and drying; over the 45-year period, temperatures have increased 1.5°C and precipitation has decreased 0.77m. The glacier retreated 280 m over the same period; unless the climate changes, the glacier will continue to loose mass and retreat.
- The glacier has retreated more than 2.35 km since 1857. The overall pattern of retreat since the end of the Little Ice Age has been interrupted twice during the period of record: one started in 1964 and lasted 5 years; the other started in 1975 and also lasted 5 years. In both cases, the glacier advanced ~100 m. Analysis of the glacier mass balance record suggests that the advance in 1964 was a result of strongly positive mass balance from 1952 and 1954, and the advance in 1975 was result of positive mass balance in 1964 and 1966. In both cases, the response time of glacier length to changes in climate was 10-12 years.
- Analyses of spatial and temporal patterns of thickness of the glacier reveal five occurrences of bulges of ice travelling as kinematic waves down the glacier. Kinematic waves occur as a result of anomalous snow accumulation; in fact, two of the documented waves appear to have started during the years of positive mass balance discussed above (K2 in 1953 and K3 in 1963). These two events were the only ones associated with glacier advance. The glacier was retreating during the other three events (K1, K4 and K5); the data are not sufficient to determine whether the rate of retreat was slowed by the passage of these kinematic waves.
- Outburst floods from Nisqually Glacier are particularly hazardous because of the proximity of the pro-glacial river to Park infrastructure. Accurate prediction of flood events is needed to mitigate the hazard. Rain-induced flooding is now well predicted from improved weather forecasts, but predicting floods induced by glacio-hydrology events remains a challenge. Ten such events have been identified over the period of record; of these events, nine occurred during periods of glacier retreat, and only one (1968) occurred during the advance related to K2 (discussed above). We have not yet identified a robust indicator of glacial-induced outburst floods but we are optimistic that emerging new high-resolution measurements of 3-D motion of the glacier will provide new insight.

Details are reported in: *Glacier Retreat, Outburst Floods, and Kinematic Waves: Nisqually Glacier Changes Related to Climate*.

An animation is at: https://drive.google.com/file/d/0B_o1CiZD1ZvcT3Y4TVdfYnRUWGs/view?usp=sharing

Glacier Retreat, Outburst Floods, and Kinematic Waves: Nisqually Glacier Changes Related to Climate

C. M. Stevens[1], H. Conway[1], P. Kennard[2], L.A. Rasmussen[1] and M.R. Koutnik[1]

1. Dept. Earth and Space Sciences, University of Washington, Seattle, WA 98195

2. Mount Rainier National Park, 55210 238th Ave E., Ashford, WA 98304

1. Introduction

Nisqually glacier, located on the southern slopes of Mt. Rainier in Washington State, USA, has a long history of observations and research; the first recorded observation of its terminus position was in 1857. Since then, numerous research efforts have maintained continuity of the long-term records, including terminus position, and measurements of ice-surface elevation across three transverse profiles. Detailed topographic maps of Nisqually glacier were produced every 5 years from 1931–1976. Daily weather observations have been made nearly continuously at the Paradise ranger station and Longmire since 1916. The National Park Service started a glacier mass balance program in 2003. The long-term records provide a unique opportunity to study how the glacier has responded to climate variability in the Pacific Northwest over the past century.

A primary objective of this report is to document the measurements of ice-surface-elevation at three different elevations across Nisqually Glacier. Measurements were started in 1931; analyses of the 84-year record provide details of spatial and temporal variations of the surface geometry that we use to track the passage of kinematic waves down the glacier. We also examine the timing of kinematic waves in context of glacier advance/retreat and the timing of outburst floods.

2. Ice-surface elevation data

The United States Geologic Survey (USGS) and Tacoma City Light began surveying ice-elevation across two transverse profiles, named P1 and P2, in late summer 1931 as a part of a project to assess the hydroelectric potential of the Nisqually River (Heliker et al., 1984). These profiles were resurveyed in 1931, 1932, 1933, 1936, and 1941. P2 was also surveyed in 1940, and surveys of a third profile (P3) started in 1942. With the exception of a few years, annual surveys of P1, P2 and P3 were continued until 1976. A fourth profile, (P2A) was surveyed from 1948–1958, but was later abandoned due to the presence of crevasses. Mean elevations of P1, P2 and P3 were ~1600 m, 1800 m, and 2000 m, respectively.

The locations of profiles changed slightly in 1976 to avoid crevasses, and they were renamed A, B, and C. In 1978 the time of surveys was changed from the fall to the spring to reduce the hazard from crevasses; spring surveys were conducted from 1978–1985. There were no surveys between 1986 and 1990. In 1991 the National Park Service (NPS) resumed fall surveys of profiles A, B and C through contracts: 1991–2002 surveys were by S. Chamberlain & Associates (SCA Consulting), Lacey, WA; there was no survey in 2000; 2003 surveys were by JVH Construction Services, Inc., Olympia, WA; and 2004–2013 surveys were by Parametrix, Lacey (later Puyallup), WA. In some years, bad weather prevented surveys of all three profiles.

In 2014, the NPS took over the annual surveying in-house. By then the glacier had retreated to a position above profile A, and a new profile (profile D) was established about 250 m up-glacier from A.

Locations of profiles are shown in Fig. 1. The profiles have been surveyed using various methods since the inception of the program in 1931. Surveying was done using a transit and stadia rod until the late 1960's and then by triangulation with a one-second-resolution theodolite (Heliker et al. 1984). Measurement details from 1984 to 2013 are not known; now they are surveyed using an electronic theodolite (total station).

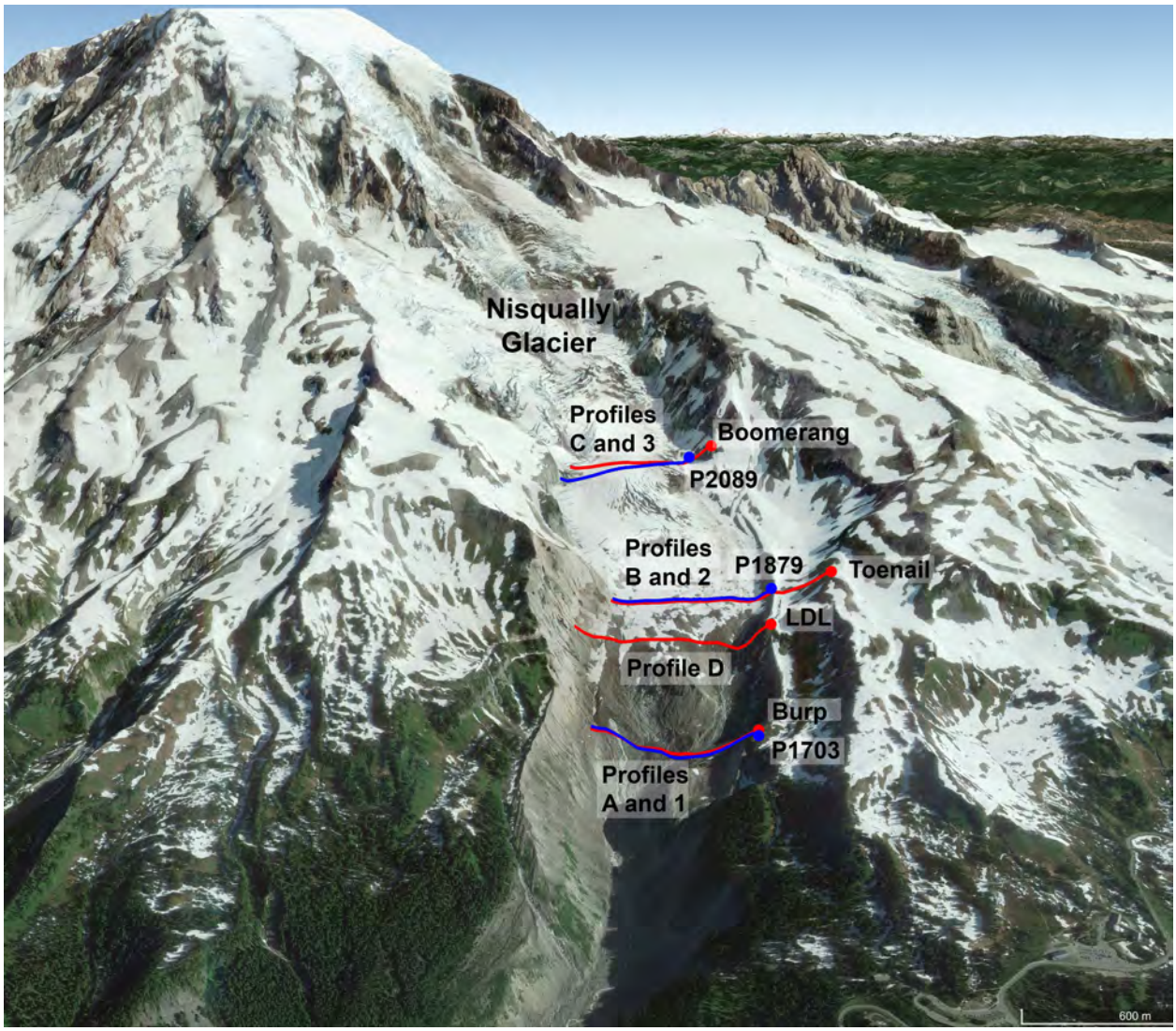

Figure 1: Locations of benchmarks and surface-elevation profiles on Nisqually Glacier. Image date: July 15, 2014.

2.1 Data collection and digitization

The digitized surface-elevation profiles derived here come from several sources:

- **1931-1979.** The original Nisqually glacier profile-elevation data were archived at the USGS Project office – Glaciology in Tacoma, WA. Unfortunately those data were lost when the Project office was closed in 1990. Mean elevations reported here for

1931–1979 are from Heliker et al. (1984). We digitized point measurements from plots of surface elevation (plates 2, 3, and 4 of Heliker et al. 1984) using a digitizing program (GraphClick), which allows users to digitize data from scanned images by counting pixels relative to the plot axes. The method introduces uncertainty that is difficult to quantify. During the period 1960–1965 (and 1931 for P1), the Heliker plates show interpolated curves of surface elevation rather than discrete data; data values reported here for those years are digitized from the curve rather than from point measurements. Again, uncertainties are difficult to quantify.

- **1980-1985.** We have not been able to locate point measurements for the profiles during this period; instead we use published mean profile elevations (Driedger and Samora, 1999; – Section 2.2).
- **1986-1990.** No surveys during this period.
- **1991-2013.** Data from contracted surveyors who distributed the measurements as CAD-generated PDF files. The measurements were not included in the final product; we have not been able to locate the raw data and here we used GraphClick and a similar software package, PlotDigitizer, to digitize the survey points from the PDF files. Due to the higher quality of the plots, the uncertainty in the digitization of the CAD-PDF files is less than that from the plates of Heliker et al. (1984). The 1998 report from SCA Consulting indicates that a surveying error caused the reported elevations for PA to be 3.79 m too high between 1991 and 1997. The data presented here are from the original CAD-generated PDF files, so we subtracted 3.79 m from the elevations derived from the 1991–1997 reports.
- **2014-present.** Data from NPS surveys

Nisqually survey point data are attached (NisquallySurveyPoints.zip).

2.2 Mean elevations of profiles

Spatially averaged elevations for each transect from 1931 to 2015 are shown in Fig. 2. Data from 1931–1979 are digitized from Heliker et al. (1984); data from 1980–1985 are from Driedger and Samora (1999); the dates of all surveys are not known, but the 1985 survey was in July (Carolyn Driedger, pers. comm., 2013). Data from 1991–2013 are digitized from the CAD-PDF files. 2014 and 2015 data are from in-house NPS measurements.

The mean elevation ($\bar{Z}(t)$) of profiles for each year 1931-1979 and 1991–2013 are calculated from:

$$\bar{Z}(t) = \frac{1}{(x_{end} - x_0)} \sum_{i=1}^{n} Z(i) \Delta x_i \qquad (1)$$

where $Z(i)$ are the elevations measured across the profile; x_0 and x_{end} are the start and end points of the profile; Δx_i is the horizontal distance between measurements; and n is the number of measurements.

Because Δx_i varies, we interpolate linearly elevations between measured points so that Δx is constant. The choice of interpolation interval Δx affects the value of $\bar{Z}(t)$. For example, for profile C during 1991–2013, decreasing Δx from 1 m to 0.1 m decreases $\bar{Z}(t)$ by an average of 4.4 m. To calculate $\bar{Z}(t)$ we used the Matlab "*trapz*" function, which is an estimate of the integral form of Eqn. 1 (i.e. Δx is small). Using $\Delta x = 0.01$ in Eqn. 1 is numerically very close to our calculated $\bar{Z}(t)$.

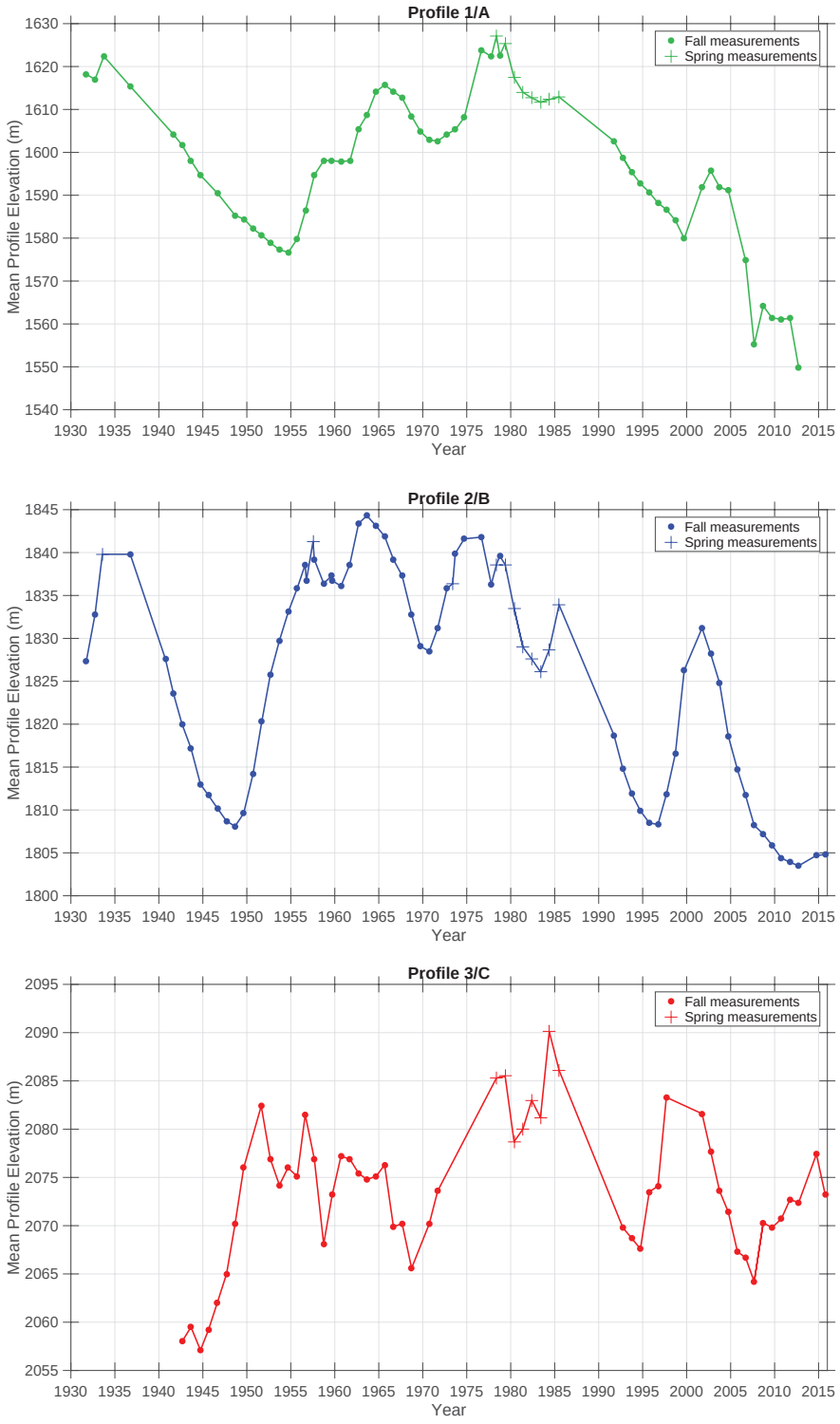

Figure 2: Time-series of mean elevations for the three transverse profiles.

Between 1931 and 1984 the length of each profile ($x_{end} - x_0$) was constant (Heliker et al., 1984). Keeping with that protocol, the 1991–2013 mean-elevation data (Fig. 2) were calculated using the same lengths; for P1/A that is from 225 m to 630 m west of "*Burp*"; for

P2/B that is 300 m to 870 m west of "*Toenail*"; for P3/C that is 90 m to 615 m west of "*Boomerang*" (see Fig. 1). If a survey did not extend to these locations, we extrapolated available measurements linearly to the original start and endpoints.

An alternative method for calculating the mean elevations is to adjust the length of the profiles each year to account for changes in the width of the glacier. However, this is a challenge because the edge of the glacier was not surveyed carefully and errors in the estimate of its location would propagate into the calculated $\bar{Z}(t)$. We compared the two methods [(i) extrapolating to the end points x_0 and x_{end} and (ii) only using the available measurements], along profile B; the average difference in $\bar{Z}(t)$ between the two methods was 0.57 m.

Calculation of $\bar{Z}(t)$ for P3/C is complicated by Wilson Glacier, which flows into the west end of the profile. For example, the 1994 P3/C survey report shows the edge of Wilson Glacier just 550 m west of Boomerang, which is east of the survey endpoint. It is likely that inter-annual variations in the thickness and dynamics of Wilson Glacier affect the elevation of the west end of P3/C. If the endpoint of P3/C is changed to 550 m in 1994, $\bar{Z}(t)$ changes by 2.4 m. Profile D has been surveyed twice (2014 and 2015); these data are not plotted here.

Details about the coordinate system, mean elevations of profiles, and uncertainties associated with the measurements are given in Appendix 2.

2.3 Spatial and temporal changes in elevation

Fig, 2 shows that mean elevations of the profiles have fluctuated on the order of 30 m over decadal time scales. Over the period of record, trends in mean elevation are: P1/A is -0.32 m/yr; P2/B is -0.24 m/yr, and P3/C is +0.06 m/yr. Trends at P1/A and P2/B are significant ($p < 0.05$), but the trend at P3/C is not. However, elevation trends between 1970 and 2015 are significant ($p < 0.05$) for all profiles: -1.38 m/yr at P1/A; -0.77 m/yr at P2/B, and -0.25 m/yr at P3/C. We chose 1970 as the start year to be consistent with recent work calculating Mt. Rainier glacier-volume loss (Sisson et al. 2011), but we acknowledge that trends depend on temporal elevation changes caused by the passage of kinematic waves (Section 3). The start year affects the trend, but Fig. 2 shows that elevations for all three profiles were near a minimum at 1970, which would minimize negative trends. Further, trends inferred from the mean profiles are consistent with thinning of Nisqually Glacier calculated by differencing digital-elevation models (DEMs) over that period (Sisson et al., 2011).

3. Kinematic waves on Nisqually Glacier

3.1 Observations

Bulges of ice travelling as kinematic waves down glaciers have been observed and modeled (Nye, 1960; van de Wal and Oerlemans, 1995). They initiate when the flux of ice into a section of a glacier exceeds the flux out (for example if there is more snow falling on the glacier). The section thickens and flows faster than the surrounding ice; the bulge of thicker ice travels down-glacier 5 to 8 times faster than the normal flow (Nye, 1960, Hooke, 2005).

In addition to the advective (horizontal) motion described above, kinematic waves have a diffusive component. Flow is proportional to the surface slope; the slope on the down-glacier side of the wave is steeper than on the up-glacier side, so in theory, the amplitude of the wave should decrease and the wavelength should increase as it progresses down glacier. In practice however, identification of kinematic waves on actual glaciers is often

hampered by the combination of diffusion and the dynamic responses of glaciers to variations in climate (van de Wal and Oerlemans, 1995).

The elevation profiles (Fig. 3) from Nisqually glacier show the passage of five bulges of ice progressing down glacier as kinematic waves. Annual elevations for each profile with the long-term (period of record) mean elevation subtracted allow comparison of the elevations on the same axes. Fig. 3 also shows a compilation of glacier length (Appendix A3) and net mass balance starting in 1949 derived from reanalysis data (see Fig. 9 in Section 4).

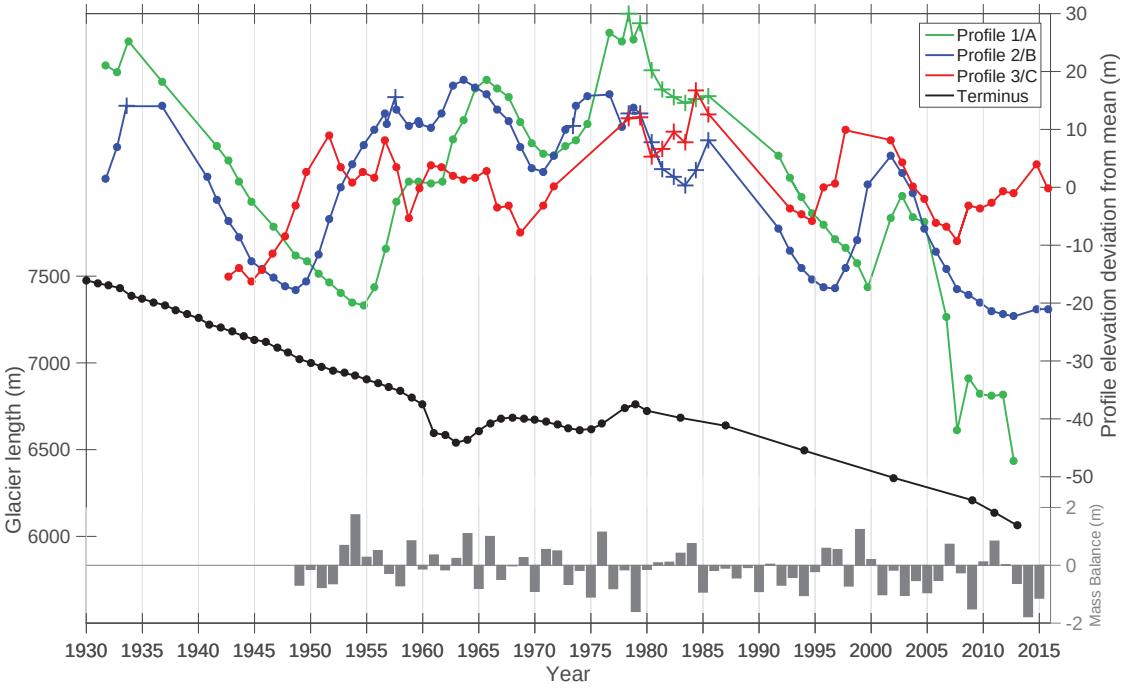

Figure 3: Mean elevations (with long-term means subtracted) of profiles, glacier length (Appendix 3) and net mass balance (from Fig. 9).

Table 1 summarizes the observations. The progression of kinematic waves can be tracked by increases in elevation first at P3/C, followed by P2/B, and then at 1/A; the onset of K1 at P3/C can be seen in 1944. Heliker et al. (1984) identified two kinematic waves (K1 and K2), and here we identify three others: K3, K4 and K5.

Other things being equal, we might expect the glacier to advance when a kinematic reaches the terminus. Veatch (1969) documented a terminus advance beginning in 1964 (Table A.1). However, the advance had already started before the crest of K2 reached the terminus (Table 1). One possibility is that the advance was a result of K1 and K2 occurring in quick succession. The amplitude of K2 was relatively small, but Fig. 3 shows that the elevation at P1 did not change between the passage of K1 and K2.

The glacier was also advancing before K3 reached the terminus, but it is was retreating when K4 and K5 reached the terminus, and it is not clear from the length-change data (Table A5.1) whether the events reduced the rate of retreat. In these cases it is possible that the strongly negative summer balance near the terminus (Fig. 10) contributed to retreat of the terminus.

	K1	K2	K3	K4	K5
P3/C front year	1944	1953	1968	1980	1994
P3/C front elevation (m)	2057.1	2074.2	2065.6	2078.7	2067.6
P3/C crest year	1951	1956	1978	1984	1997
P3/C crest elevation (m)	2082.4	2081.5	2085.3	2090.1	2083.3
P3/C amplitude (m)	25.3	7.3	19.7	11.4	15.7
P2/B front year	1948	1960	1971	1983	1997
P2/B front elevation (m)	1808.1	1836.1	1831.2	1826.1	1811.8
P2/B crest year	1957	1963	1974	1985	2001
P2/B crest elevation (m)	1839.2	1844.3	1841.6	1833.9	1831.2
P2/B amplitude (m)	31.1	8.2	10.4	7.8	19.4
P1/A front year	1954	1962	1972	1983	1999
P1/A front elevation (m)	1576.7	1605.4	1604.2	1611.7	1579.9
P1/A crest year	1958	1965	1976	1985	2002
P1/A crest elevation (m)	1598.1	1615.7	1623.8	1612.9	1595.7
P1/A amplitude (m)	21.4	10.3	19.6	1.2	15.8
Front velocity: P3–P2 (m/yr)	267.5	152.8	356.7	356.7	356.7
Front velocity: P2–P1 (m/yr)	125	375	750	N/A	375
Crest velocity: P3–P2 (m/yr)	178.3	152.9	-267.5	1070	267.5
Crest velocity: P2–P1 (m/yr)	750	375	375	N/A	750
Length change (year)	-38(1959)	+44(1966)	+46(1977)	-11(1986)	-18(2003)

Table 1: Summary of data relating to five kinematic waves (K1, K2, K3, K4 and K5). Identifiers in the left column refer to the profile (e.g. P3/C); **front year** is the year the kinematic wave first reached that profile; **front elevation** is the mean profile elevation for that year; **crest year** is the year that the elevation peaked at each profile; **crest elevation** is the mean profile elevation for that year; **amplitude** is the difference between the front elevation and crest elevation. **Front** and **crest velocities** between P3 and P2 and between P2 and P1 are calculated by dividing the distance between the profiles by the time taken for the front or crest to move between profiles. **Length change (year)** is the glacier-length change (m/yr) the year *after* the crest of the kinematic wave passed P1/C.

3.2 Glacier-flow model

To further investigate kinematic waves on Nisqually glacier we adapted a 1-D glacier-flow-line model (Oerlemans, 2001), which has also been used to investigate glacier response to Late-Holocene climate in the Pacific Northwest by Roe and O'Neal (2009). The model consists of the continuity equation and simplified equations of motion solved on a finite-difference grid. Bed topography comes from ice-penetrating radar soundings (Driedger and Kennard, 1986). We adjusted the sliding and deformation parameters in the model to best-fit observations of glacier length, thickness and surface velocity.

We do not expect to reconstruct all details of the glacier dynamics: the model physics are simplified and neither variations in the width of the glacier nor the influx of ice from Wilson Glacier are considered. The bed geometry is based on sparse data and is likely different from the actual bed topography. Although we can adjust model parameters to produce realistic thicknesses and velocities, errors in one parameterization may compensate for errors in another.

Despite these limitations, the model is useful for exploring the response of Nisqually Glacier to potential changes in climate. Model experiments included using precipitation and temperature data from Longmire Ranger station, with calibrated lapse rate and melt-rate factors, to model the glacier-average melt. The melt is subtracted from the winter

precipitation to calculate mass balance. Although variations in mass balance derived in this way correlate well (r = 0.68) with the history derived from upper-air data (Section 4), the amplitude of the balances are an order of magnitude larger.

In this experiment we spun up the model using long-term mean values of temperature and precipitation, and then used the precipitation and temperature data from 1915 to 2015 as input to the model.

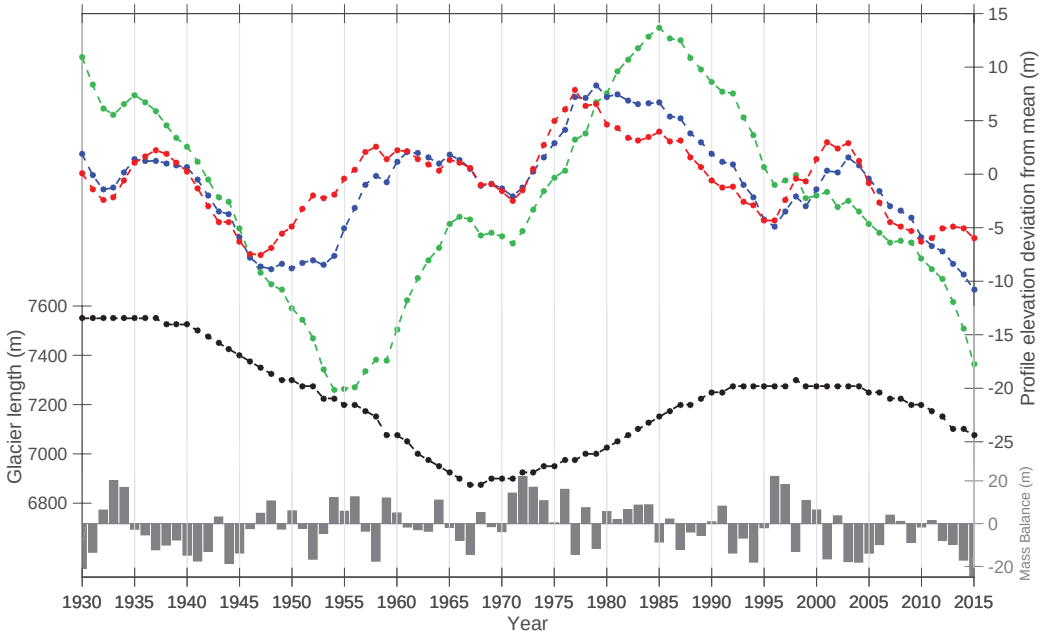

Figure 4: Modeled mean elevations (with long-term means subtracted) of profiles, glacier length, and annual mass balance from 1930 to 2015. Profile color scheme is the same as Fig. 3.

Results in Fig. 4 show that modeled profile elevations starting in 1930 are broadly similar to observations (Fig. 3). A kinematic wave starts to pass through P3/C in 1946, P2/B in 1948–1950, and P1/A in 1955. Another wave passes through in the 1970's. Modeled wave amplitudes are similar to the observations. However the model does not predict the observed decrease in surface elevation in the early 1970's and the increase in the early 2000's at P1/A. The model simulates glacier length quite well until about 1980; in more recent years it is too long.

We also conducted experiments to investigate the response of Nisqually glacier to perturbations in climate. We spun up the model to an equilibrium state with an equilibrium-line altitude (ELA) of 2600 m. We then perturbed the mass balance by lowering the ELA by 100 m for one year (Experiment 1); raising the ELA by 100m for one year (Experiment 2); raising the ELA by 100 m for one year and lowering the ELA by 100 m (below the steady-state ELA) the following year (Experiment 3); and allowing the ELA to fluctuate around the mean value by adding noise from a normal distribution (sigma = 100 m) (Experiment 4).

Results of Experiments 1, 2 and 3 are shown in Fig. 5. The panels show modeled elevations at profiles C B and A, glacier length, and mass balance. For Experiment 1 (blue), lowering ELA (with associated positive mass balance) created a kinematic wave. The maximum

amplitude at P1/A was 3 meters, or about 7.5% of the modeled glacier thickness (40 m), consistent with kinematic-wave theory. The wave took longer to pass through profile A due to diffusion of the wavelength and amplitude of the wave.

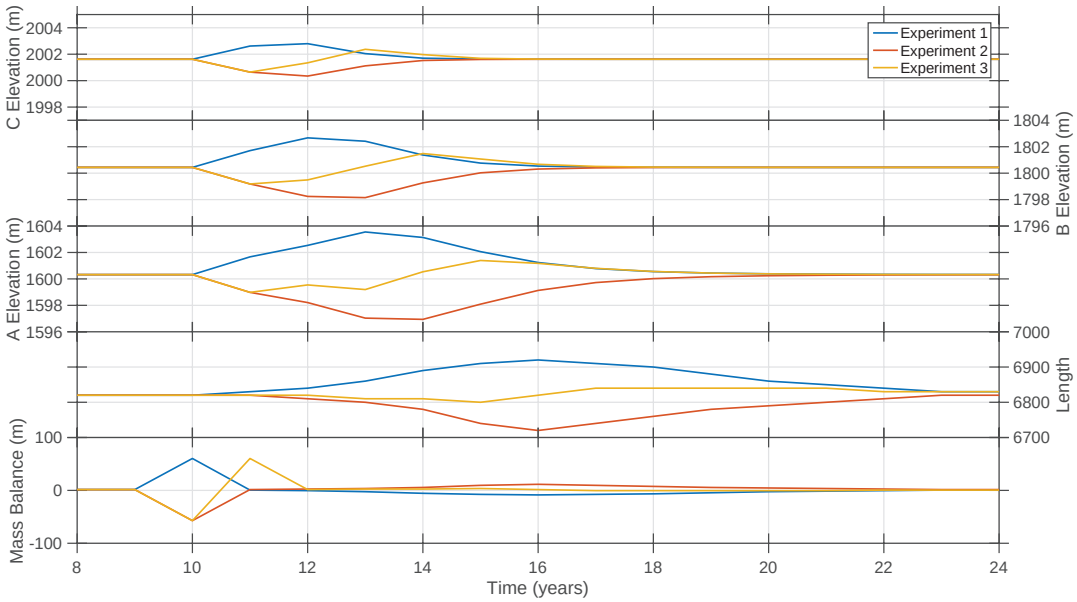

Figure 5: Modeled glacier response to three mass-balance perturbations. Panels show, from top to bottom, modeled elevations at profiles C, B, and A; glacier length; and three prescribed mass-balance perturbations.

Interestingly, the negative-mass-balance perturbation introduced in Experiment 2 (red) produced a similar result to Experiment 1 but with opposite (negative) amplitude. The shape of the trough is slightly different because the upslope side of the trough has a steeper gradient whereas the wave in experiment 1 has a steeper gradient on the downslope side of the wave. In all cases the effect of the perturbations on glacier mass balance and length had vanished after about 13 years (Fig. 5).

Fig. 6 shows results from Experiment 4. The mass-balance fluctuations caused surface elevations to rise and fall. The magnitude of these deviations is notably larger than in Experiments 1, 2, and 3. The frequencies of the profile elevations are damped compared to the mass-balance fluctuations because the surface elevation and flux passing a profile is the cumulative sum of several years of mass-balance history affecting the flow of ice, which has non-linear dynamics.

The four experiments show that the passage of the peak of the bulge (or the minimum of the trough) is delayed for several years after the mass-balance perturbation. In contrast, the experiment using the climate data (Fig. 3) showed very little or no time delay between mass-balance anomalies and surface-elevation change. This may be due to the different ways mass balance is calculated between the experiments. Regardless, in all experiments, the peaks or lows passed profile C first, then B and finally A. These experiments suggest that the kinematic waves observed on Nisqually glacier are a natural part of the system and are caused by inter-annual variability in mass balance. Negative-mass-balance-anomaly years are capable of producing troughs and positive-mass-balance-anomaly years can produce crests. The profile-elevation deviations that are observed are an integration of

several years of glacier history. In Experiments 1, 2, and 3, the profile elevations returned to their steady configuration after 10 years or less, which suggests that longer-term changes over multiple decades can be interpreted as the response to climate forcing.

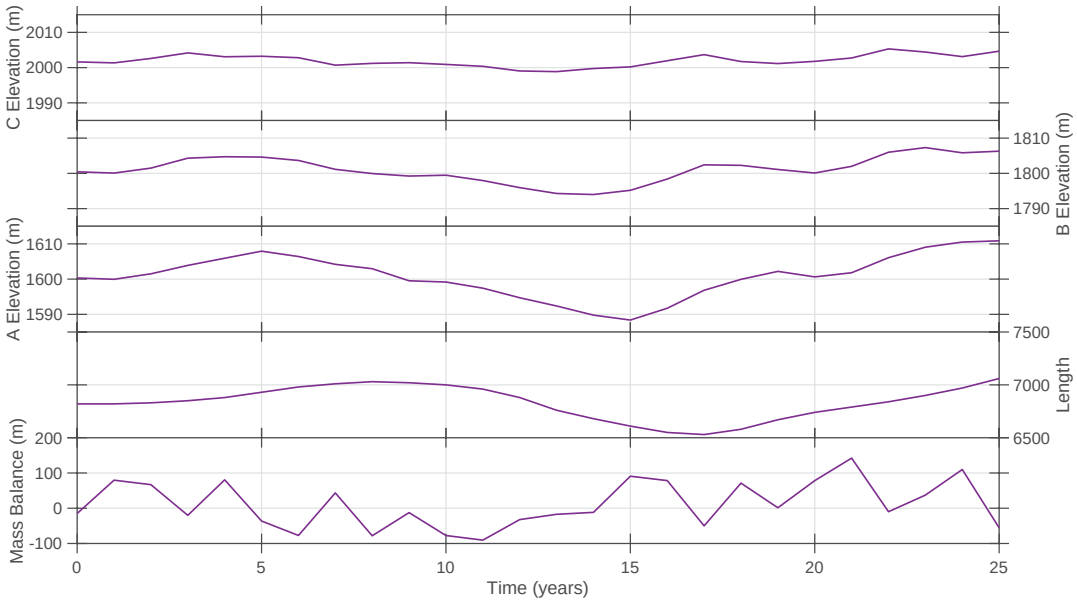

Figure 6: Modeled glacier response to prescribed random fluctuations in annual mass balance. Panels show, from top to bottom, modeled elevations at Profiles C, B, and A, modeled glacier length, and the synthetic-mass-balance variations used in the experiment.

We also conducted an experiment in which the ELA was increased by 100 m over 30 years, but interspersed by a single-year 200-m ELA lowering at year 10. In this case, the terminus retreated until the kinematic wave produced by the strongly positive mass balance anomaly at year 10 moved down glacier causing an advance. The glacier then continued to retreat.

4. Nisqually Glacier mass balance

4.1 Model calibration

4.1.1 Surface balance measurements

The NPS began collecting vertical profiles of surface mass balance in 2002 using a network of stakes set on the glacier (Table A4.1) and Fig. 7 shows the measurements of winter balance b_w and summer balance b_s at different elevations on Nisqually glacier between 2002 and 2012. The $b_s(z)$ profiles show an increasing trend with altitude (that is, becoming less negative), apart from irregularities around 1900 m, which might have been caused by debris cover and/or observational inconsistencies. On the other hand, the $b_w(z)$ profiles do not show a consistent trend. To a first approximation, they are almost constant with elevation, with inter-annual values ranging from about 2 m to 4 m (water equivalent w.e.).

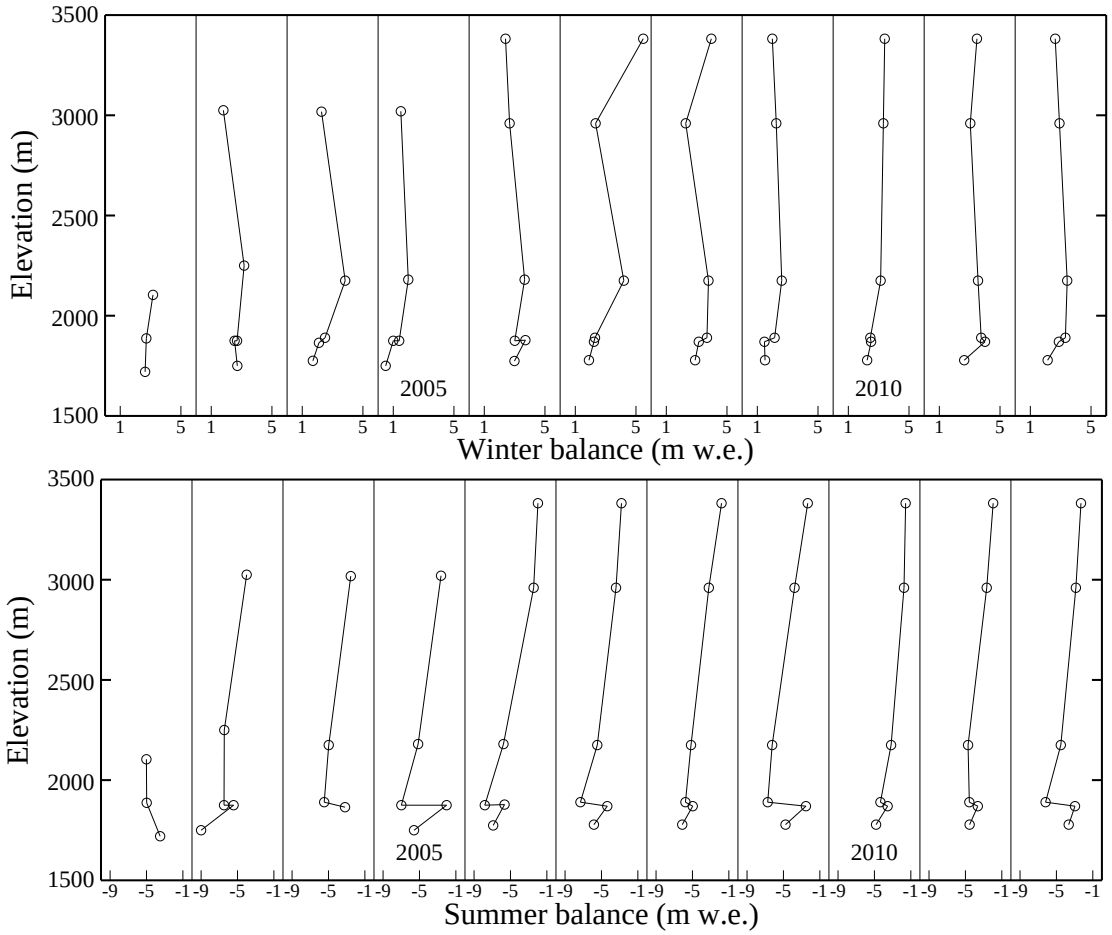

Figure 7: Time series (2002-2012) of measured vertical profiles of: **upper panel,** winter mass balance $b_w(z)$; **lower panel,** summer balance $b_s(z)$ in meters water equivalent (m w.e.)

The summer-balance measurements are used to calibrate a positive-degree-day (PDD) model (de Woul and Hock, 2005; Rasmussen and Wenger, 2009). In the model, $b_s(z)$ is estimated by interpolating $T(z)$ profiles in the NCEP-NCAR Reanalysis database (Kistler et al., 2001) and T^+ is the accumulated total of positive daily temperatures (°C) at each elevation. Summer balance from 1700m to 3382m is estimated from:

$$b_s^* = -4.35T^+ - 0.85 \qquad (2)$$

with rms error 0.65 m w.e., and $r = -0.93$ ($r^2 = 0.87$).

The winter-balance measurements are used to calibrate a moisture flux model (Rasmussen and Conway, 2003). In the model, precipitation on the glacier is assumed to be proportional to the moisture flux at the 850mbar level. The moisture flux is $U\mathrm{RH}_{850}$ where RH_{850} is the relative humidity $0 \leq \mathrm{RH}_{850} < 1$, and $U = \vec{V}\cos(\phi_{850} - \phi')$, where $\vec{V}$ is the wind speed (m/s) and ϕ_{850} is the wind direction at the 850mbar level.

The critical direction for the moisture flux $\phi' = 186^o$ was determined empirically using precipitation measurements from Paradise. Values for $b_w(z)$ were calculated by assuming precipitation falls as snow when $T(z) \leq 2$°C. Using the measurements for calibration, winter balance is estimated from:

$$b_w^* = 2.51U - 2.45 \quad (3)$$

with $r = 0.88$ ($r^2 = 0.77$).

The correlations for estimating b_s^* and b_s^* using the upper-air Reanalysis data are remarkably high, giving confidence to estimate glacier mass balance back to 1948 when the Reanalysis database started.

4.2 1948–2015 Nisqually Glacier-average annual mass balance B_a

Applying the relation of Eqn (2) to the $T(z)$ profiles in the Reanalysis database over 1948-2015 and integrating the resulting $b_s(z)$ over the area-altitude distribution for Nisqually glacier (Fig. 8), produces the glacier-average summer surface balance $B_s(t)$.

Similarly, applying the method of Eqn (3) with the October–May 186° Reanalysis winds and integrating the resulting $b_s(t)$ over the area-altitude distribution of the glacier produces an estimate of the glacier-average winter balance $B_w(t)$.

The glacier-average annual balance is the algebraic sum of the two components: $B_a(t) = B_w(t) + B_s(t)$.

The components and sum of the glacier-average mass balance are shown in Fig. 9.

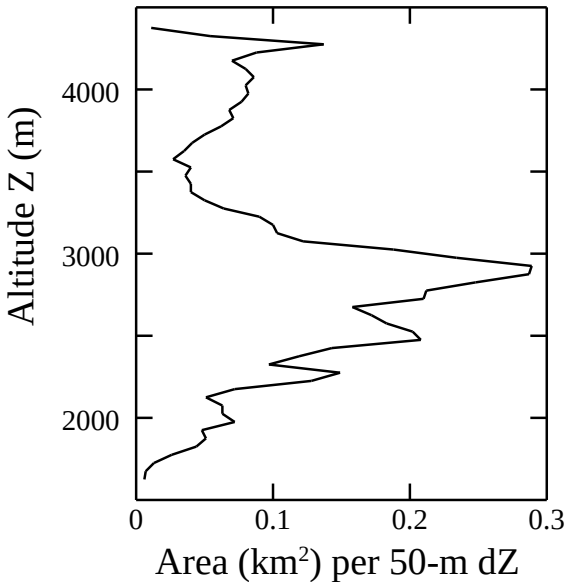

Figure 8: Nisqually area-altitude distribution.

There was an abrupt increase of summer sea surface temperature (SST) in the northeast Pacific in 1989 (Hare and Mantua, 2000), which is evident in the summer balance, which became more negative by 0.38 m at that time (Fig. 9 – upper panel). Although there is no significant trend in the winter balance (Fig. 9 – middle panel), the annual balance shows a change from being slightly negative (-0.1 m) prior to 2000, to strongly negative (-0.49 m) after 2000. According to the Student's statistical t-test, the probability that samples before and after the shift are from the same population is less than 0.026.

4.3 1917 – 2015 Nisqually Glacier summer balance b_s at 1655 m

The long-term records of temperature and precipitation from Longmire and Paradise allow for extension of the surface mass balance record back to 1917. Because Paradise is near the altitude of the Nisqually terminus, it is a better record for modeling Nisqually glacier mass balance because it avoids making an explicit assumption about the temperature lapse rate dT/dz between Longmire and the glacier.

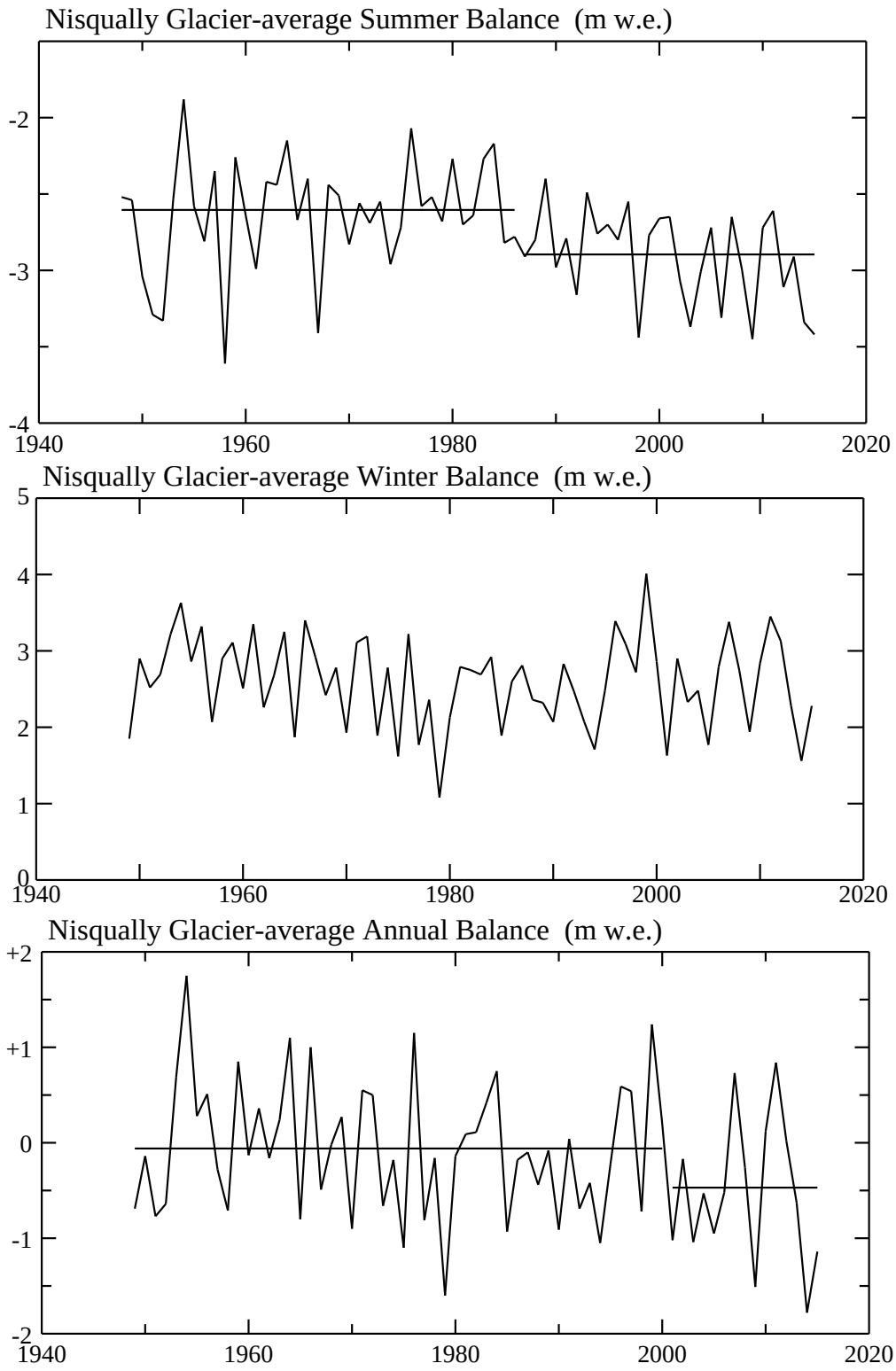

Figure 9: 1948-2015 Glacier-average surface summer balance B_s (**upper panel**), winter balance B_w (**middle panel**), and annual balance B_a (**lower panel**). Glacier-averaged balances are modeled using upper air data, which started in 1948 (Kistler et al. 2001), and the area-altitude distribution (Fig. 8), calibrated with observations (Section 4.1).

Although the published Paradise T record is less complete than the one for Longmire, we filled in the Paradise record using Longmire. For each of the months June–September, daily maximum temperature $T_{\max}$ at Longmire (842m) and Paradise (1655m) are strongly correlated positively. The mean differences over 1917–2015 for these months were 6.8, 6.7, 6.3, 5.9 °C with Longmire warmer. We use the summer (June-September) Paradise $T_{\max}$, with observations missing there filled in by applying those differences, to estimate surface summer balance b_s at that altitude.

Applying the $b_s(T)$ relation of Eqn (2) to the extended Paradise $T(t)$ record yields the $b_s(t)$ shown in Fig. 10. The mean 2002–2015 b_s is 1 m/yr more negative than during the 1959–1985 period. According to Student's statistical t-test, probabilities that the samples before and after each shift are from the same population are very small (0.000, 0.012, 0.006), respectively, for the 1958, 1985, and 2001 shifts.

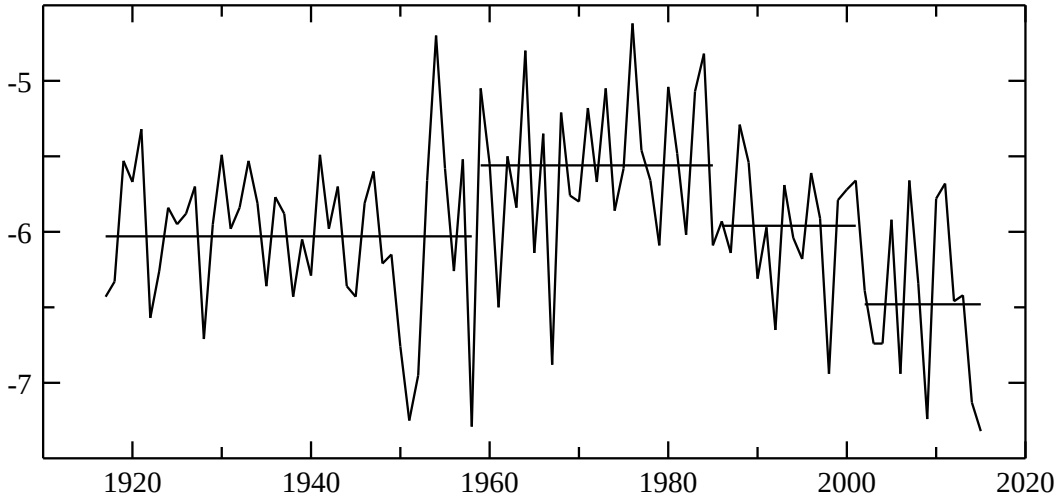

Figure 10: Surface summer balance $b_s(t)$ m a^{-1} w.e at 1655 m a.s.l. 1917–2015 estimated from Eqn. 2 and summer temperature measurements from Paradise, with missing data filled-in where necessary with measurements from Longmire.

Not surprisingly, results of summer balance from near the terminus show more structure than the glacier-wide estimates using the upper-air data (Figure 9, **upper panel**). Both show a step change between 1985 and 1986 (-0.3 m glacier wide, -0.5m at 1655m). The positive change (+0.6 m at 1959) at 1655 m is not apparent in the glacier-wide summer balance record, and nor is the negative change (-0.6 m at 2001). Interestingly, the timing of the negative change in summer balance at 1655 m (-0.6 m at 2001) coincides with a negative change (-0.5 m) in the glacier average annual balance (Fig. 9, **lower panel**).

5. Climate trends at Paradise (1665m a.s.l)

We extracted historical monthly temperature and precipitation data for Paradise from the National Climatic Data Center. The record started in January 1916. We analyzed the data for monthly, seasonal, and annual trends. The accumulation season is defined as October through May and the melt season as June through September. Fields considered include total precipitation (m of water equivalent), total snowfall (m), extreme maximum and minimum temperatures, mean-daily-minimum and mean-daily–maximum temperature (°C), averaged over months, seasons, and years, and monthly, seasonal, and annual mean

daily temperature (°C). Several trends significant at the 95% confidence level were found over the entire period of record (1917–2015), and over the period 1970 to 2015. Significant trends ($p<0.05$) are shown in Table 2. Caution is needed when interpreting trends because missing data (specially prior to 1948), changes in station location (e.g Paradise moved in 1970) and changes in instrumentation (changes from manual to automated measurements) can bias the analyses.

Variable	Season or Annual	Period	Trend (per yr)
Annual mean maximum temperature (°C)	Annual	1917 - 2015	-0.013
Seasonal mean minimum temperature (°C)	Melt	1917 - 2015	+0.011
Total precipitation (m)	Accumulation	1917 - 2015	+0.012
Total snowfall (m)	Accumulation	1917 - 2015	+0.080
Mean daily maximum temperature (°C)	Accumulation	1917 - 2015	-0.015
Mean daily minimum temperature (°C)	Accumulation	1917 - 2015	+0.013
---	---	---	---
Total precipitation (m)	Annual	1970 - 2015	-0.017
Total snowfall (m)	Annual	1970 - 2015	-0.097
Mean daily maximum temperature (°C)	Annual	1970 - 2015	+0.029
Mean daily minimum temperature (°C)	Annual	1970 - 2015	+0.037
Mean daily temperature (°C)	Annual	1970 - 2015	+0.033
Extreme minimum temperature (°C)	Annual	1970 - 2015	+0.097
Total snowfall (m)	Melt	1970 - 2015	-0.007
Mean daily maximum temperature (°C)	Melt	1970 – 2015	+0.044
Mean daily minimum temperature (°C)	Melt	1970 - 2015	+0.038
Mean daily temperature (°C)	Melt	1970 - 2015	+0.041
Extreme minimum temperature (°C)	Accumulation	1970 - 2015	+0.091
Mean daily minimum temperature (°C)	Accumulation	1970 - 2015	+0.0365
Mean daily temperature (°C)	Accumulation	1970 - 2015	+0.029

Table 2: Summary of significant ($p < 0.05$) seasonal and annual trends in temperature and precipitation at Paradise (1665 m a.s.l.)

Trends since 1970 indicate warming and drying; the mean daily temperature has *increased* 1.5°C and annual precipitation has *decreased* by 0.77 m over the 45-year period. The pattern of warming and drying is consistent with the total 4.37 m *decrease* in snowfall over the past 45 years. The trends suggest that the glacier will continue to retreat, unless the climate changes.

There was no significant trend in the day of year of snow-melt-out from Paradise, defined here as the first day of the year when snow depth at Paradise is recorded as zero. For this statistic, we require that there be consecutive days of zero snow depth to correct for data errors (e.g. there are several times in the record that sandwich a zero recording between measurements of over 100 cm). The average melt-out-date since 1920 is day 191 (July 10).

6. Debris cover and stagnant ice

Supra-glacial debris exerts strong influence on mass balance; a thin cover of debris enhances melting, but debris thicker than 20-50mm insulates the underlying ice (Driedger, 1981; Reznichenko et al., 2010; Nicholson and Benn, 2013; Lejeune et al. 2013; Reid and Brock, 2014). The spatial variability of debris thickness and evolution adds complexity to the problem of predicting how debris-covered glaciers respond to climate change (e.g., Benn et al., 2012).

Stagnant ice and detachment of a portion of the glacier occurs when supra-glacial debris insulates and inhibits melting of the glacial ice cover while the active portion of the glacier retreats. In the case of non-debris-covered glaciers, the mass balance monotonically decreases from zero at the equilibrium line altitude to its most negative value at the terminus. In the case of the debris being thick enough to insulate the glacier, the mass balance decreases to a minimum some distance up-glacier from the terminus and then increases again towards the debris-covered terminus. With ongoing thinning and retreat of the active portion of the glacier, the debris-covered stagnant ice becomes detached and melts in place.

Data analyzed in this report do not explicitly show that the terminus has stagnated, although the apparent rapid (-165m/yr) retreat from 1960 to 1961 (Table A5.1 in Appendix 5) suggests that stagnant ice was present at the terminus for some time prior to 1960. In addition, others have shown that it has been stagnant in the past (Heliker et al., 1984) and it is likely stagnant today (Allstadt et al. 2015).

7. Outburst floods and debris flows

Floods, including outburst floods and debris flows are relatively common and have been observed and documented in Mt. Rainier National Park (Driedger and Fountain, 1989, Walder and Driedger, 1995; Copeland, 2010; Skloven-Gill and Fountain, 2015). Many of the floods in the park are related to extreme rain events in the fall, and are especially damaging when freezing levels are high. For example on Nov 6-7, 2006, more than 450mm of rain fell in 36 hours causing widespread damage to roads, trails and buildings that exceeded $36 million.

Parker (2009) analyzed debris-flow producing storms for Mt. Rainier and found they are characterized by high freezing levels and little snow on the ground, implying that precipitation fell as rain rather than snow on bare ground at high elevations. All debris flows on Mt Rainier during the period 2001 to 2006 initiated from elevations above 1800m.

7.1 Outburst floods, kinematic waves, and glacier length changes

The potential hazard from the Nisqually River during events such as November 2006 is particularly high because of its proximity to Longmire and the Sunshine Point campground, and also because of its impact on the road and main utilities lines to Longmire and Paradise. The hypsometry and geometry of the basin also contributes: rain falling in the catchment region is likely diverted rapidly to the bed of the glacier and focused in the confined outlet channel. Such extreme precipitation can also destabilize steep-angle saturated sediments adjacent to the glacier resulting in debris flows. Table 3 gives a summary of documented outburst floods and debris flows from Nisqually Glacier.

Month	Day	Year	Estimated peak discharge	Weather conditions
Oct		1926	>100-200 $m^3 s^{-1}$	Occurred during first heavy rain at end of summer
Oct	14	1932	>100-200 $m^3 s^{-1}$	No rain from Sep 25 to Oct 9. 220mm rain Oct 10-14
Oct	24	1934	>100-200 $m^3 s^{-1}$	252mm rain Oct 20-22
Oct	1	1947	>100-200 $m^3 s^{-1}$	1500mm rain at Paradise, Oct 2
Oct	25	1955	2000 $m^3 s^{-1}$	96mm rain in previous 32 h
Jun	2	1968	<83 $m^3 s^{-1}$	112mm rain in 24 h
Jul	4	1970	85 $m^3 s^{-1}$	Dry
Jul	14	1972	140-170 $m^3 s^{-1}$	63 mm rain
Jun	22	1986	>1.7 $m^3 s^{-1}$	40 mm rain in previous month
Oct	27	2012	Peak of 4.8 ft on the Nisqually River gauge at Longmire; the gauging station at National had a peak of 70$m^3 s^{-1}$ and 19 $m^3 s^{-1}$ increase in 15 min.	66 mm rain at Paradise in previous 12 h accompanied by warming temperatures; likely rain on snow event

Table 3. Nisqually Glacier outburst flood and debris flow history compiled from Driedger and Fountain (1989) and an NPS press release for the Oct 27, 2012 event (see https://www.nps.gov/mora/learn/news/glacial-outburst-flood.htm), USGS gauging station data, and Northwest Weather and Avalanche Center data.

Of interest is to determine whether the glaciological record can provide insight into the timing of outburst floods, which might prove useful for mitigating the hazard from floods. Benn et al. (2012) reviewed debris-covered glaciers in the Himalaya and discussed glacial hydrology and outburst floods in that regime. They suggested that englacial drainage systems usually drain supraglacial melt water efficiently, but on low-angle glaciers (<10°) drainage pathways can close, allowing water to pond in cavities near the surface. It is possible that voids on stagnant-ice areas of Nisqually Glacier are water filled during the summer, but we are unaware of observations to confirm or discount this possibility.

As discussed above, although the rapid 165-m terminus retreat from 1960 to 1961 (Table A3.1) suggests significant loss of glacier ice at that time, the observations (Table 3) do not indicate an outburst flood then. Most documented outburst floods occurred during years of glacier retreat; five occurred when the rates of retreat were greater than the long-term average (-15m/yr), but the other five occurred when retreat-rates were less than -15m/yr, and one (June 2, 1968) occurred during a time of glacier advance.

We examined the timing of outburst floods with the passage of kinematic waves down the glacier (Table 1). We consider the year *after* the crest of the wave reaches P1, the profile closest to the terminus (Fig. 1). Of the five kinematic waves detected in our analysis, two are possible candidates: the timing of K2 (amplitude 10.3 m) in 1966 precedes the documented outburst flood in 1968 by one year, and the timing of K4 (amplitude 1.2 m) in 1986 is coincident with the 1986 flood. K2 was likely a result of strongly positive (up to +1.8m/yr) mass balance between 1952 and 1954 (Fig. 9, lower panel); the crest of the kinematic wave had passed P3 in 1957 and P2 in 1963 (Table 1). The glacier started to advance in 1964 and was still advancing in 1968 (Table A3.1); if this interpretation is

correct, the response time of the glacier length to the mass balance perturbation was 10-12 years. The glacier retreated (-10m) between 1968 and 1969, but it is not clear whether the outburst flood contributed to the retreat. Nor is it clear that the kinematic wave and glacier advance contributed to the outburst flood.

The cause and effects of K4 is less clear; a positive (1.1m/yr) mass balance in 1976 (Fig. 9 lower panel) is a possibility, but this is 4 years before the kinematic wave was first detected at P3, and 8 years before the crest of the wave passed through P3. The glacier was retreating (-11m/yr) when the outburst flood in 1986.

The glacier advanced 102 m from 1975 to 1979 (Table A5.1). Assuming the response to mass balance perturbations is the same as the response to the 1964 advance (10-12 years), it is possible that the strongly positive mass balances in 1964 (+1m/yr) and 1966 (+0.9m/yr) contributed to cause the advance.

8. Future work

Continued measurements of surface elevation and surface mass balance, as well as temperature and precipitation, are important for understanding how Nisqually Glacier will respond to ongoing environmental changes. The measurements are especially important to maintain because of the existing long-term historical record.

Recent advances in remote sensing instruments and technology allow collection of data at high spatial and temporal resolution. Several of these techniques have been tested and proven on glaciers in the Pacific Northwest and Mt Rainier (e.g. Sisson et al. 2011; Allstadt et al. 2015; Shean, 2013). Instruments and methods include:

- "Structure from Motion" (SfM) aerial, UAV, and ground-based photogrammetry. This low-cost technique provides 3-D information of an object or surface (structure) using photographs acquired from multiple viewpoints (motion). High-resolution (<10 cm) digital elevation models (DEMs) from repeat surveys are differenced to detect 3-D motion (Shean, 2013; Immerzeel et al. 2014).
- Terrestrial LiDAR (TLS) offers rapid data acquisition with ~1-2 cm accuracy at ranges up to 4 km. It produces point cloud data, which can be used to create DEMs with ~5-30 cm/px spatial resolution; repeat measurements can be used to track 3-D surface motion.
- High-resolution (~0.3-1.0 m/px) archived commercial satellite imagery (WorldView) can now be accessed using the NASA Ames Stereo Pipeline (Shean et al., 2016). After correction and co-registration, relative horizontal and vertical DEM accuracy over glacier surfaces is ~0.2-0.5 m (Shean et al. 2016), which is sufficient to resolve spatially-coherent sub-meter elevation changes.

Targeted, high-resolution studies of 3-D motion using remote sensing data will likely offer new insight into kinematic waves and the hydrology and dynamics of glaciers that produce outburst floods (c.f. Allstadt et al., 2015). Such studies would also elucidate details of how the debris cover thickness is changing, and how the changes influence the formation of stagnant ice and outburst floods.

9. Conclusions

Climate records from Longmire and Paradise (1917-2015) and glaciological data from Nisqually Glacier starting in 1857 provide a unique opportunity to examine the response of Nisqually Glacier to climate over the past century. The climate records indicate warming

and drying over the period 1970 – 2015; over this time, temperatures have increased 1.5°C and precipitation has decreased 0.77m. The glacier has retreated more than 2.35 km since 1857. Unless the climate changes, the glacier will continue to retreat.

The overall pattern of retreat has been interrupted twice during the period of record: one started in 1964 and lasted 5 years; the other started in 1975 and also lasted 5 years. In both cases, the glacier advanced a little more than 100m. Analysis of the glacier mass balance record suggests that the advance in 1964 was a result of strongly positive mass balance from 1952 and 1954, and the advance in 1975 was result of positive mass balance in 1964 and 1966. In both cases, the response time of glacier length to changes in climate was 10-12 years.

Analyses of spatial and temporal patterns of thickness of the glacier reveal five occurrences of bulges of ice travelling as kinematic waves down the glacier. Kinematic waves occur as a result of anomalous mass balance; in fact two of the documented waves appear to have started during the years of positive mass balance discussed above (K2 in 1953 and K3 in 1963). These two events were the only ones associated with glacier advance. The glacier continued to retreat during the other three events (K1, K4 and K5); the data are not sufficient to determine whether the rate of retreat was slowed by the passage of these kinematic waves.

Outburst floods from Nisqually Glacier are particularly hazardous because of the proximity of the pro-glacial river to Park infrastructure. Accurate prediction of flood events is needed to mitigate the hazard. Rain induced flooding is now well predicted from improved weather forecasts, but predicting floods induced by glacio-hydrology events remains a challenge. Ten such events have been identified over the period of record; of these events, nine occurred during periods of glacier retreat, and only one (1968) occurred during the advance related to K2 (discussed above). We have not yet identified a robust indicator of glacial-induced outburst floods. We are optimistic that emerging new high-resolution measurements of 3-D motion of the glacier (discussed in Section 8) will provide insight.

10. Acknowledgements

This study was supported and funded by Task Agreement # **P12AC15072** by and between the National Park Service (NPS) and University of Washington (UW), issued against the Pacific Northwest Cooperative Ecosystem Studies Unit (PNW CESU) Cooperative and Joint Venture Agreement, H8W07110001. We also thank Paul Kennard (Rainier National Park) for initiating the project and partnering with us on the study.

Harvey Greenburg (UW Earth and Space Sciences), Amir Sheikh (UW Civil and Environmental Engineering), and Mark Stoemer and Hunter Hadaway (UW Center of Environmental Visualization), worked with Max Stevens to produce the Nisqually Glacier animation: https://drive.google.com/file/d/0B_o1CiZD1ZvcT3Y4TVdfYnRUWGs/view?usp=sharing

11. References

Allstadt, K.E., D.E. Shean, A. Campbell, M. Fahnestock and S.D. Malone, 2015. Observations of seasonal and diurnal glacier velocities at Mount Rainier, Washington, using terrestrial radar interferometry, *The Cryosphere*, *9*(6), 2219–2235, doi:10.5194/tc-9-2219-2015.

Benn, D.I., T. Bolch, K. Hands, J. Gulley, A. Luckman, L.I. Nicholson, D. Quincey, S. Thompson,

R. Toumi and S. Wiseman, 2012. Response of debris-covered glaciers in the Mount Everest region to recent warming , and implications for outburst flood hazards, *Earth Sci. Rev.*, *114*(1-2), 156–174, doi:10.1016/j.earscirev.2012.03.008.

Copeland, E.A. 2010. Recent Periglacial Debris Flows from Mount Rainier, Washington. M.S. Thesis, Oregon State University, 125p.

De Woul, M. and R. Hock. 2005. Static mass-balance sensitivity of Arctic glaciers and ice caps using a degree-day approach. *Ann. Glaciol.*, 42, 217–224.

Driedger, C.L., 1981, Effects of ash thickness on snow ablation, in Lipman, P.W. and Mullineaux, D.R., eds., The 1980 eruptions of Mount St. Helens, Washington: *U.S. Geological Survey Professional Paper* 1250, pp. 757-760.

Driedger, C.L. and A.G. Fountain, 1989. Glacier outburst floods at Mount Rainier, Washington State, U.S.A. *Ann. Glaciol.*, *13*, 51–55.

Driedger, C.L. and P. Kennard, 1986. Ice Volumes on Cascade Volcanoes: Mount Rainer, Mount Hood, Three Sisters, Mount Shasta, *Available from Supt Doc, USGPO, Wash DC 20402.*

Driedger, C.L. and B. Samora, 1999. Surface Altitude Measurements at Nisqually Glacier, Mount Rainier, WA 1931-1998, in *Proceedings of Mount Rainier Centennial Symposium*, UW Press, Seattle, WA.

Hare, S.R., and N.J. Mantua, 2000. Empirical evidence for North Pacific regime shifts in 1977 and 1989, *Prog. Oceanogr.*, *47*(2-4), 103–145, doi:10.1016/S0079-6611(00)00033-1.

Heliker, C., A. Johnson and S. Hodge, 1984. The Nisqually Glacier, Mount Rainier, Washington, 1857 - 1979: A summary of the long-term observations and a comprehensive bibliography, *USGS Open-file Rep. 83-541 1984. 20 p, 4 Figures.*

Hooke, R.L. 2013. *Principles of Glacier Mechanics*.

Immerzeel, W.W., P.D.A. Kraaijenbrink, J.M. Shea, A.B. Shrestha, F. Pellicciotti, M.F.P. Bierkens and S.M. de Jong, 2014. High-resolution monitoring of Himalayan glacier dynamics using unmanned aerial vehicles. *Remote Sens. Environ.*, **150**, 93–103.

Kistler, R. and 12 others. 2001. The NCEP/NCAR 50-year reanalysis: monthly means CD-ROM and documentation. Bull. Am. Meteorol. Soc., 82(2), 247–267.

Lejeune, Y., J-M. Bertrand, P. Wagnon and S. Morin, 2013. A physically based model of the year-round surface energy and mass balance of debris-covered glaciers, *J. Glaciol,* **59**, 327-344.

Lighthill, M.J. and G.B. Whitham, 1955. On Kinematic Waves. I. Flood Movement in Long Rivers, *Proc. R. Soc. A Math. Phys. Eng. Sci.*, *229*(1178), 281–316, doi:10.1098/rspa.1955.0088.

Nicholson, L. and D.I. Benn, 2013. Properties of natural supraglacial debris in relation to modeling sub-debris ablation. *Earth Surf. Process. Landforms* **38**, 490–501.

Nye, J.F. 1960. The Response of Glaciers and Ice-Sheets to Seasonal and Climatic Changes, *Proc. R. Soc. A Math. Phys. Eng. Sci.*, *256*(1287), 559–584, doi:10.1098/rspa.1960.0127.

Oerlemans, J. 2001. *Glaciers and climate change*, CRC Press.

Parker, L. 2009. Meteorological conditions associated with rain-related periglacial debris flows on Mount Hood, Oregon and Mount Rainier, Washington. M.S. Thesis, Oregon State University, 88p.

Paterson, W.S.B. 1981. The physics of glaciers, 2nd end,

Rasmussen, L.A. and H. Conway, 2003. Using upper-air conditions to estimate South Cascade Glacier (Washington, U.S.A.) summer balance. *J. Glaciol*., 49(166), 456-462.

Rasmussen, L.A. and J.M. Wenger, 2009. Upper-air model of summer balance on Mount Rainier, USA, *J. Glaciol.*, *55*(192), 619–624, doi:10.3189/002214309789471012.

Reid, T. and B.W. Brock, 2014. Assessing ice-cliff backwasting and its contribution to total ablation of debris-covered Miage glacier, Mont Blanc massif, Italy. *J. Glaciol.* 60(219)**,** 3-13.

Reznichenko, N., T. Davies, J. Shulmeister, and M. McSaveney, 2010. Effects of debris on ice-surface melting rates: an experimental study, *J. Glaciol.*, *56*(197), 384–394.

Roe, G.H. and M.A. O'Neal, 2009. The response of glaciers to intrinsic climate variability: observations and models of late-Holocene variations in the Pacific Northwest. *J. Glaciol.*, *55*(193), 839–854.

Sisson, T.W. J.E. Robinson and D.D. Swinney, 2011. Whole-edifice ice volume change A.D. 1970 to 2007/2008 at Mount Rainier, Washington, based on LiDAR surveying. *Geology*, *39*(7), 639–642, doi:10.1130/G31902.1.

Shean, D.E. 2013. Quantifying Mass Balance in the WA Cascades, IGS Northwest Glaciologists Meeting, Burnaby, BC. Canada.

Shean, D.E., O. Alexandrov, Z. Moratto, B.E. Smith, I.R. Joughin, C.C. Porter and P.J. Morin, 2016. An automated, open-source pipeline for mass production of digital elevation models (DEMs) from very high-resolution commercial stereo satellite imagery, *ISPRS J. Photogramm. Remote Sens*, 116, 101-117, doi: 10.1016/j.isprsjprs.2016.03.012.

Skloven-Gill, J. and A.G. Fountain, 2015. *Glacier change, kinematic waves, and outburst floods at Nisqually Glacier, Mountain Rainier, Washington*.

Veatch, F.M. 1969. Analysis of a 24-year photographic record of Nisqually Glacier, Mount Rainier National Park, Washington, *Geol. Surv. Prof. Pap.*, iv, 52 p.

van de Wal, R. and J. Oerlemans, 1995. Response of valley glaciers to climate change and kinematic waves: a study with a numerical ice-flow model. *J. Glaciol.*, *41*(137).

10. APPENDICES

A1. Link to animation: *Response of Nisqually Glacier to climate variations over the past century:*

https://drive.google.com/file/d/0B_o1CiZD1ZvcT3Y4TVdfYnRUWGs/view?usp=sharing

A2. Coordinates, measurement uncertainty, and mean elevation of profiles

UTM coordinates (UTM Zone 10, NAD27) have been calculated for points for all years that profile data are available. For some years, interpolated curves of surface elevation rather than discrete data were available. In these cases we digitized point values from the curve rather than from point measurements. We include these points so that they can be imported into a Geographic Information System (GIS).

Heliker et al. (1984) did not report bearings for the original profiles P1, P2, & P3, and we have not been able to locate them elsewhere. We estimated the bearings from a high-resolution scan of Plate 1 from Heliker et al. (1984). We used Adobe Photoshop to measure the angles between the profiles and a line between two known locations (*Toenail* and *Boomerang*) in order to calculate the bearings. Bearings for profiles A, B, and C are given in the 1991–2013 survey reports.

To estimate the uncertainty with the Photoshop angle-measuring method, we assume that the profiles are printed accurately on the map. Bearings calculated for profiles A, B, and C by this method are: S61.178°E; S77.845°E; S86.033°E, respectively. Bearings given in the 1991-2013 survey reports for the same profiles are: S61.612°E; S77.84°E; S85.76°E. To quantify the uncertainty in the bearings, we consider a point on profile A 500 m from the endpoint, *Burp*. The difference in eastings between the two bearings is 3.3 m and the difference in northings is 1.9 m; we conclude that our Photoshop method for estimating the bearing is adequate given other uncertainties in the measurements.

Additional uncertainty comes from 1991-1997 measurements of profile A. In 1998 the surveyors realized that they had been using reference point (*P1703*) instead of *Burp*. The successive drawings do not report the bearing for the 1991–1997 measurements but the 2013 report indicates that the 1991–1997 profiles started at *Burp* and followed bearing S 61.612° E; the 1998 – 2006 and 2008 – 2013 profiles started at *Y2K* and followed bearing S 56.135° E; the 2007 profile started at *Y2K* and followed bearing S 61.612° E.

In summary, calculation of coordinates of profiles were done as follows for:

- Profile 1 (1931–1975) we use endpoint *P1703* with bearing S56.135°E.
- Profile A (1976–1985) we use endpoint *Burp* with bearing S61.612°E.
- Profile A (1991–1997) we use endpoint *P1703* with bearing S61.612°E.
- Profile A (1998–2006) we use endpoint *Y2K* with bearing S56.135°E.
- Profile A (2007) we use endpoint *Y2K* with bearing S61.612°E.
- Profile A (2008-2013) we use endpoint *Y2K* with bearing S56.135°E.
- Profile 2 we use endpoint *P1879* with bearing S77.845°E.
- Profile B we use endpoint *Toenail* with bearing S77.845°E.
- Profile 3 we use endpoint *P2089* with bearing S83.149°E.
- Profile C we use endpoint *Boomerang* with bearing S85.764°E.
- Profile D we use endpoint *LDL* with bearing S72.534°E.

Sources of measurement error for the profile elevations include: (i) uncertainty with the surveying method. Heliker et al. (1984) reports the accuracy of the transit and stadia rod measurements of ±0.3 m. Accuracy of measurements with the one-second theodolite is ±0.03 m. Accuracy of modern total-stations is about ±0.01 m at 1-km range; (ii) uncertainties from small-scale surface roughness, and estimating the thickness of supra-glacial debris. During the surveys, the theodolite is fixed at a known location and a surveyor places a stadia rod with prism on the glacier surface; the total station measures the distance and angle to the prism. The location of the prism (and thus the glacier surface by knowing the distance between the prism and the end of the rod) is calculated. However, if the end of the rod is not on bare ice, as is often the case on the debris-covered lower Nisqually Glacier), the thickness of the debris must be estimated by probing through the debris to the ice surface below. Estimates of the error due to debris thickness have not been reported in the past. For example, the 1995 report indicates "±7 feet of debris cover", and "areas of heavy debris", but it is not clear how these values were estimated.

The surveys performed by contract (1991-2013) report a range of debris thicknesses over a section of the profile, but it is not clear whether the reported ice-surface elevations account for the debris cover. Here we assume that the reported elevations do have the debris thickness subtracted and the reported value is the ice-surface elevation.

The 1978–1985 surveys took place in the spring when the ice was covered in snow. For those years, surveyors probed to find the snow thickness and assumed that the probes were stopped by the previous ablation season's surface. Heliker et al. (1984) estimated the uncertainty due to the spring snow cover to be ±0.25 m.

Historically, ice-surface elevations have been reported as the mean elevation for each profile; Table A2.1 is a compilation of these data. Because a finite number of points are surveyed across the profiles, the roughness of the glacier surface introduces uncertainty in the calculation of the mean elevation. For example, if surveyors chose local highs as sample points as they traversed the glacier, the calculated mean elevation would be biased high. Additional uncertainty in the calculated mean elevations comes from the changing width of the glacier. Calculating the mean elevation requires integrating the surface-elevation measurements over the width of the glacier, but changes of the margins of the glacier have not been measured accurately. Surveying the location of the glacier margin is not trivial due to the amount of debris on the lower Nisqually Glacier; the transition from active, debris-covered glacier ice to moraine is not always well defined.

Profile 1/A:

Month	Day	Year	Mean Elevation
_	_	1931	1618.2
_	_	1932	1617
_	_	1933	1622.4
_	_	1936	1615.4
8	26	1941	1604.2
8	21	1942	1601.7
8	26	1943	1598.1
9	18	1944	1594.7

Month	Day	Year	Mean Elevation
9	13	1973	1605.3
9	18	1974	1608.1
9	4	1976	1623.8
10	18	1977	1622.3
5	20	1978	1627.1
10	4	1978	1622.6
5	15	1979	1625.4
_	_	1980	1617.4

9	11	1946	1590.4	_	_	1981	1614
9	2	1948	1585.3	_	_	1982	1612.7
9	22	1949	1584.4	_	_	1983	1611.7
9	15	1950	1582.2	_	_	1984	1612.3
9	5	1951	1580.7	_	_	1985	1612.9
9	9	1952	1578.9	_	_	1991	1600.5
9	10	1953	1577.3	_	_	1992	1598.5
9	22	1954	1576.7	_	_	1993	1593.6
9	22	1955	1579.8	_	_	1994	1591.2
9	6	1956	1586.5	10	1	1995	1589.6
9	5	1957	1594.7	9	26	1996	1589.3
10	3	1958	1598.1	9	10	1997	1592
8	29	1959	1598.1	9	22	1998	1583.1
9	18	1960	1597.8	9	23	1999	1579.3
9	26	1961	1598.1	10	2	2001	1588.5
9	8	1962	1605.4	9	24	2002	1600.9
8	29	1963	1608.7	9	29	2003	1598.2
9	13	1964	1614.2	9	27	2004	1593.3
9	1	1965	1615.7	9	12	2006	1585
8	30	1966	1614.2	9	6	2007	1566
8	30	1967	1612.7	9	15	2008	1575
9	26	1968	1608.4	9	15	2009	1573.8
10	6	1969	1604.8	10	6	2010	1568
9	28	1970	1602.9	9	29	2011	1564.4
9	14	1971	1602.6	9	26	2012	1557.1
9	27	1972	1604.2				

Profile 2/B:

Month	Day	Year	Mean Elevation	Month	Day	Year	Mean Elevation
_	_	1931	1827.3	10	4	1972	1835.8
9	30	1932	1832.8	5	30	1973	1836.4
7	31	1933	1839.8	9	12	1973	1839.9
_	_	1936	1839.8	9	18	1974	1841.6
_	_	1940	1827.6	9	2	1976	1841.8
8	26	1941	1823.6	10	18	1977	1836.3
8	21	1942	1820	5	20	1978	1838.6
8	26	1943	1817.2	10	4	1978	1839.6
9	24	1944	1813	5	15	1979	1838.6
8	22	1945	1811.7	_	_	1980	1833.5
8	28	1946	1810.2	_	_	1981	1829

9	11	1947	1808.7	_	_	1982	1827.6
8	31	1948	1808.1	_	_	1983	1826.1
8	22	1949	1809.6	_	_	1984	1828.7
9	15	1950	1814.2	_	_	1985	1833.9
9	14	1951	1820.3	_	_	1991	1818.8
9	5	1952	1825.8	_	_	1992	1814.7
9	11	1953	1829.7	_	_	1993	1814.9
9	20	1954	1833.1	_	_	1994	1810.4
9	19	1955	1835.8	10	1	1995	1809.3
8	21	1956	1838.6	9	26	1996	1808.9
10	7	1956	1836.7	9	10	1997	1811.8
7	12	1957	1841.3	9	22	1998	1815.9
9	3	1957	1839.2	9	23	1999	1825.6
9	27	1958	1836.4	10	2	2001	1830.1
8	30	1959	1837.3	9	24	2002	1828
10	2	1959	1836.7	9	29	2003	1824.7
9	16	1960	1836.1	9	27	2004	1818.2
9	14	1961	1838.6	10	11	2005	1814.6
9	17	1962	1843.4	9	12	2006	1812.5
8	27	1963	1844.3	9	6	2007	1809.6
9	12	1964	1843.1	9	15	2008	1807.1
8	31	1965	1841.9	9	15	2009	1806.4
8	31	1966	1839.2	10	6	2010	1805
8	28	1967	1837.3	9	29	2011	1804.1
9	24	1968	1832.8	9	26	2012	1803.5
9	15	1969	1829.1	10	2	2014	1805.1
9	28	1970	1828.5	10	5	2015	1805.6
9	14	1971	1831.2				

Profile 3/C:

Month	Day	Year	Mean Elevation	Month	Day	Year	Mean Elevation
8	24	1942	2058	5	19	1978	2085.3
8	26	1943	2059.5	5	14	1979	2085.5
9	24	1944	2057.1	_	_	1980	2078.7
8	22	1945	2059.2	_	_	1981	2080
8	22	1946	2062	_	_	1982	2083
9	12	1947	2065	_	_	1983	2081.2
9	1	1948	2070.2	_	_	1984	2090.1
8	24	1949	2076	_	_	1985	2086.1
8	22	1951	2082.4	_	_	1992	2072.1

9	4	1952	2076.9	_	_	1993	2073.4
9	14	1953	2074.2	_	_	1994	2072
9	4	1954	2076	10	1	1995	2075.2
9	23	1955	2075.1	9	26	1996	2078.5
8	22	1956	2081.5	9	10	1997	2085
9	4	1957	2076.9	10	2	2001	2076.5
9	27	1958	2068.1	9	24	2002	2075.9
9	17	1959	2073.2	9	29	2003	2072.9
9	14	1960	2077.2	9	27	2004	2070.7
9	19	1961	2076.9	10	11	2005	2067.4
9	20	1962	2075.4	9	12	2006	2067.6
8	28	1963	2074.8	9	6	2007	2068
9	10	1964	2075.1	9	15	2008	2072.1
8	30	1965	2076.3	9	15	2009	2071.5
9	1	1966	2069.9	10	6	2010	2073.1
8	29	1967	2070.2	9	29	2011	2074.7
9	25	1968	2065.6	9	26	2012	2079.5
9	29	1970	2070.2	10	2	2014	2078
9	13	1971	2073.6	10	5	2015	2072.9

Profile D:

Month	Day	Year	Mean Elevation
10	2	2014	1742.2
10	5	2015	1741.2

Table A2.1 Dates and mean elevations of profiles. Data for profiles 1/A, 2/B and 3/C are plotted in Fig. 2. Measurements on 1/A were discontinued after 2012; profile D was established in 2014.

A3. Terminus position

Lt. August V. Kautz made the first recorded observation of the terminus position in 1857. Occasional measurements (see Heliker et al., 1984) of the terminus were made until 1918, when the NPS began annual surveys of its position. The Conservation District took over these surveys in 1960, until 1966 when the USGS Project office – Glaciology in Tacoma took over. The USGS continued the measurements at least through 1979 (Heliker et al., 1984). Calculated changes (m/yr) are negative for retreat, positive for advance; the glacier has been retreating steadily since 1857, interrupted by an advance of 146 m from 1964 to 1968 and another of 102 m from 1975 to 1979. Total glacier retreat since 1857 is 2.35 km The Portland State University glacier group has used numerous sources to compile a consistent length-history (Skloven-Gill and Fountain, 2015).

Year	Length (km)	Change (m/yr)
1857	8.412	
1885	8.180	-8
1892	8.137	-6
1905	7.905	-18
1908	7.907	1
1910	7.874	-17
1918	7.737	-17
1919	7.720	-18
1920	7.705	-14
1921	7.673	-32
1922	7.653	-20
1923	7.640	-13
1924	7.615	-25
1925	7.593	-22
1926	7.567	-26
1927	7.554	-13
1928	7.527	-27
1929	7.511	-16
1930	7.475	-36
1931	7.460	-15
1932	7.445	-15
1933	7.432	-13
1934	7.385	-47
1935	7.369	-16
1936	7.349	-20
1937	7.332	-17
1938	7.305	-27
1939	7.279	-26
1940	7.258	-21
1941	7.220	-38
1942	7.203	-17
1943	7.179	-24
1944	7.155	-24
1945	7.133	-23
1946	7.120	-12
1947	7.086	-34
1948	7.059	-27
1949	7.021	-38
1950	7.001	-20
1951	6.979	-22
1952	6.956	-23
1953	6.941	-15
1954	6.927	-14
1955	6.903	-24
1956	6.883	-20
1957	6.860	-23
1958	6.836	-24
1959	6.798	-38
1960	6.760	-38
1961	6.595	-165
1962	6.586	-9
1963	6.540	-46
1964	6.557	17
1965	6.609	52
1966	6.653	44
1967	6.678	25
1968	6.686	8
1969	6.676	-10
1970	6.670	-6
1971	6.659	-11
1972	6.644	-15
1973	6.622	-22
1974	6.614	-8
1975	6.618	4
1976	6.648	30
1978	6.739	46
1979	6.761	22
1980	6.724	-37
1983	6.683	-14
1987	6.638	-11
1994	6.495	-20
2002	6.338	-20
2009	6.209	-18
2011	6.139	-35
2013	6.064	-37

Table A3.1 History of length and changes of Nisqually Glacier 1857 to 2013. [*Table adapted from Skloven-Gill and Fountain, 2015*].

A4. Stake measurements of glacier mass balance

	2003	2004	2005	2006	2007	2008	2009	2010	2011	2012	2013	2014
Stake 1				(1a)	(1)	(1)	(1)	(1)	(1)	(1)	(1)	(1)
Elev (m)	NA	NA	NA	3382	3382	3382	3382	3392	3393	3382	3403	3387
bw	NA	NA	NA	2.40	5.48	3.97	1.99	3.40	3.40	2.64	2.49	2.48
bs	NA	NA	NA	-1.98	-2.80	-1.80	-2.33	-1.57	-1.91	-2.30	-3.34	-2.20
bn	NA	NA	NA	0.41	2.68	2.17	-0.34	1.83	1.49	0.34	-0.85	0.28
Stake 2	(1)	(1)	(1)_	(1)	(2)	(2)	(2)	(2)	(2)	(2)	(2)	(2)
Elev(m)	3025	3018	3020	2960	2960	2960	2960	2958	2958	2958	2958	2959
bw	1.80	2.27	1.50	2.67	2.34	2.28	2.25	3.31	2.97	2.92	3.13	2.96
bs	-3.99	-2.55	-2.63	-2.45	-3.40	-3.20	-3.78	-1.75	-2.60	-2.86	-4.43	-3.35
bn	-2.19	-0.27	-1.13	0.22	-1.06	-0.92	-1.53	1.56	0.37	0.06	-1.30	-0.39
Stake 3												
Elev (m)	2250	2175	2180	2180	2175	2175	2175	2172	2172	2171	2171	2179
bw	3.17	3.83	1.99	3.66	4.20	3.78	2.61	3.13	3.48	3.43	3.21	3.60
bs	-6.45	-4.97	-5.15	-5.77	-5.46	-5.16	-6.24	-3.17	-4.64	-4.52	-6.09	-5.28
bn	-3.28	-1.14	-3.16	-2.11	-1.26	-1.38	-3.64	-0.05	-1.16	-1.10	-2.88	-1.68
Stake 4												
Elev (m)	1875	1890	1875	1875	1890	1890	1890	1890	1859	1859	1859	1859
bw	2.70	2.50	1.39	3.01	2.30	3.68	2.14	2.45	3.61	3.31	3.37	3.19
bs	-6.48	-5.47	-6.99	-7.82	-7.31	-5.77	-6.73	-4.34	-4.41	-6.19	-7.51	-6.28
bn	-3.78	-2.98	-5.60	-4.81	-5.01	-2.09	-4.58	-1.89	-0.80	-2.89	-4.14	-3.10
Stake 4A												
Elev (m)	1875	1865	1875	1878	1870	1870	1870	1856	1856	1858	1852	1856
bw	2.54	2.10	1.00	3.71	2.23	3.14	1.47	2.50	3.85	2.88	4.35	3.10
bs	-5.43	-3.18	-2.02	-5.65	-4.36	-4.97	-2.53	-3.55	-3.49	-2.99	-3.70	-3.79
bn	-2.89	-1.07	-1.01	-1.94	-2.13	-1.83	-1.06	-1.05	0.36	-0.11	0.64	-0.68
Stake 5												
Elev(m)	1750	1775	1750	1774	1778	1778	1778	1757	1757	1758	1758	1759
bw	2.72	1.70	0.50	2.99	1.90	2.90	1.51	2.24	2.59	2.14	2.35	2.43
bs	-9.00	NA	-5.60	-6.90	-5.83	-6.12	-4.77	-4.82	-4.48	-3.36	-4.07	-5.45
bn	-7.85	NA	-5.09	-3.92	-3.92	-3.22	-3.26	-2.57	-1.89	-1.22	-1.72	-3.02

Table A4.1 Summary of stake measurements of mass balance on Nisqually Glacier, started by NPS in 2003. For each stake, bw is winter balance; bs is the summer balance and bn is the annual balance, all in m/year [*Table adapted from NPS report, 2015*].